The ribosomal maturation factor P from *Mycobacterium smegmatis* facilitates the ribosomal biogenesis by binding to the small ribosomal protein S12

Received for publication, February 8, 2018, and in revised form, October 15, 2018 Published, Papers in Press, November 8, 2018, DOI 10.1074/jbc.RA118.002298

Tinyi Chu[‡1], Xing Weng[‡1], Carmen Oi Kwan Law[‡1], Hoi-Kuan Kong[‡1], Jeffrey Lau[‡], Sheila Li[‡], Hoa Quynh Pham[‡], Rui Wang[‡], Liang Zhang[‡], Richard Y. T. Kao[§], Kwok-Fai Lau[¶], Jacky Chi Ki Ngo[¶2], and Terrence Chi Kong Lau[‡3]

From the [‡]Department of Biomedical Sciences, City University of Hong Kong, Kowloon, Hong Kong, China, the [§]Department of Microbiology, Hong Kong University, Hong Kong, China, and the [¶]School of Life Sciences, Chinese University of Hong Kong, Hong Kong, China

Edited by Karin Musier-Forsyth

The ribosomal maturation factor P (RimP) is a highly conserved protein in bacteria and has been shown to be important in ribosomal assembly in *Escherichia coli*. Because of its central importance in bacterial metabolism, RimP represents a good potential target for drug design to combat human pathogens such as *Mycobacterium tuberculosis*. However, to date, the only RimP structure available is the NMR structure of the ortholog in another bacterial pathogen, *Streptococcus pneumoniae*. Here, we report a 2.2 Å resolution crystal structure of MSMEG_2624, the RimP ortholog in the close *M. tuberculosis* relative *Mycobacterium smegmatis*, and using *in vitro* binding assays, we show that MSMEG_2624 interacts with the small ribosomal protein S12, also known as RpsL. Further analyses revealed that the conserved residues in the linker region between the N- and C-terminal domains of MSMEG_2624 are essential for binding to RpsL. However, neither of the two domains alone was sufficient to form strong interactions with RpsL. More importantly, the linker region was essential for *in vivo* ribosomal biogenesis. Our study provides critical mechanistic insights into the role of RimP in ribosome biogenesis. We anticipate that the MSMEG_2624 crystal structure has the potential to be used for drug design to manage *M. tuberculosis* infections.

Ribosomes account for a large portion of cell mass, and their synthesis can be highly energy-consuming. It is estimated that in rapidly growing *Escherichia coli*, around 90% of the energy consumption is for protein synthesis, and a significant amount is used for generating ribosomes (1). The complete 70S bacterial ribosome is composed of the 30S small subunit and the 50S large subunit. In general, the 30S small subunit consists of the 16S rRNA and 21 ribosomal proteins (S1–S21); the 50S large subunit consists of the 23S and 5S rRNAs and 36 ribosomal proteins (L1–L36). Although active ribosomes can be reconstituted *in vitro* using individually purified ribosomal proteins and rRNAs, the process occurs at a much slower rate and requires harsher conditions (2). By contrast, *in vivo* ribosomal biogenesis is assisted by various ribosomal cofactors, including helicase, chaperones, maturation factors, and GTPase, and hence needs a lower activation energy and produces fewer intermediates (3).

The ribosomal maturation factor P (RimP), also known as yhbC, is a highly conserved ribosomal cofactor in both Gram-negative and Gram-positive bacteria (Fig. S1, *A–C*). Null mutation of RimP in *E. coli* shows slower growth than WT at high temperatures (4). In the food-borne pathogen *Salmonella enteritidis*, the RimP mutant shows decreased growth rate and becomes more sensitive to both reactive oxygen and nitrogen intermediates but less virulent *in vitro* (5). In the Gram-positive pathogen *Streptococcus pneumoniae*, the null mutant is lethal (6). Overall, these phenotypic studies highlight the physiological importance of RimP in bacteria.

Several mechanistic studies have showed the functional association of RimP with ribosomal biogenesis. Wikström and coworkers (4) found that the RimP null mutant reduced the levels of polysome and mature 70S, whereas it increased the amounts of 30S and 50S in *E. coli*. Moreover, less accumulation of 30S than 50S was observed in polysome profiling (4). In their study, RimP was only found in the fractions of 30S subunit but not others in sucrose gradient centrifugation, and primer extension studies demonstrated that RimP knockout bacteria up-regulated the level of pre-16S rRNA but down-regulated mature 16S rRNA levels (4). Recently, quantitative MS studies on *E. coli* suggested that RimP can increase the binding kinetics of the S5 and S12 ribosomal proteins to the 5′ domain of rRNA *in vitro* (7). In addition, it was reported that the relative timing of the assembly of the 3′ domain and the formation of the central pseudoknot structure in the 16S rRNA depend on the presence of the assembly factor RimP (8). These *in vivo* and *in vitro* data indicate that RimP is essential for the biogenesis of the 30S small subunit in *E. coli*.

Despite extensive biochemical and biophysical study, the mechanism of RimP in ribosomal biogenesis is still not fully understood. The only available structure to date is the solution

This work was supported by General Research Fund (GRF) 11101518, 9042616, and 21101917 and Health and Medical Research Fund (HMRF) Grant 15140342. The authors declare that they have no conflicts of interest with the contents of this article.

This article contains Table S1 and Figs. S1–S8.

The atomic coordinates and structure factors (code 5GL6) have been deposited in the Protein Data Bank (http://wwpdb.org/).

[1] These authors contributed equally to this work.

[2] To whom correspondence may be addressed. E-mail: jackyngo@cuhk.edu.hk.

[3] To whom correspondence may be addressed. E-mail: chiklau@cityu.edu.hk.

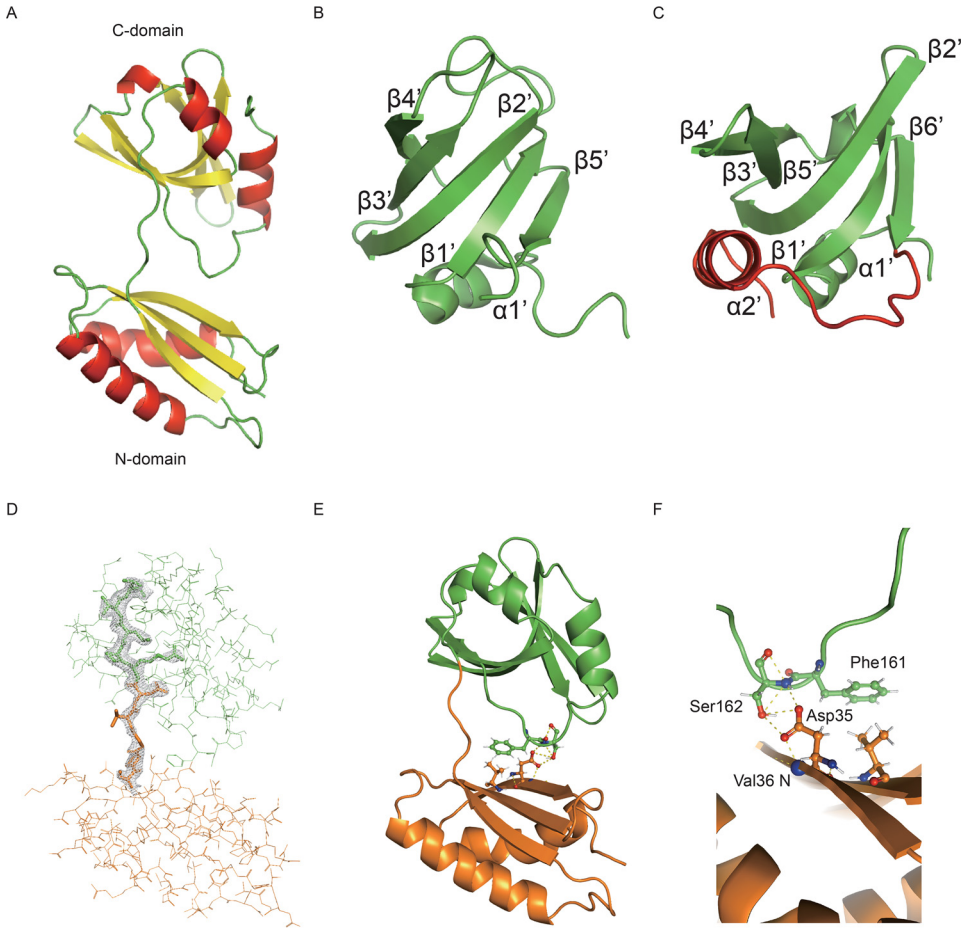

Figure 1. The crystal structure of MSMEG_2624. *A*, the *cartoon colors* the structure of MS- MEG_2624 by secondary structure. *B* and *C*, comparison between the C-terminal domain of SP14.3 (*B*) and that of MSMEG_2624 (*C*). The additional α helix and the long connecting loop in MSMEG_2624 are highlighted in *red*. *D*, electron density of the interdomain linker, at 2.0σ level. *E* and *F*, residues participate in the interdomain interaction. Hydrogen bond interactions are highlighted using *yellow dashed lines*.

structure of SP14.3, an ortholog in *S. pneumoniae*, solved using NMR. It consists of a highly negatively charged N-terminal domain and a slightly positively charged C-terminal domain resembling the Sm fold (6). Because of the flexible linker between the two domains, their relative orientation is not defined. The structure, however, is limited in clarifying its mechanism in ribosomal biogenesis.

Mycobacterium tuberculosis is the causative agent of tuberculosis, which killed 1.7 million people in 2016 (9). Active *M. tuberculosis* infection leads to severe pulmonary and occasionally extrapulmonary symptoms, particularly in immunocompromised patients, such as those with HIV. Moreover, the emergence of multidrug-resistant strains confounds effective treatment, which typically involves prolonged use of multiple antibiotics. Therefore, the discovery of a druggable target in *M. tuberculosis* is of importance in future drug development. Here, we describe the crystal structure of RimP homolog MSMEG_2624 in *Mycobacterium smegmatis*, a model organism for studying *M. tuberculosis*. We demonstrate that the linker region of MSMEG_2624 plays an important physiological role in interacting with RpsL, the small ribosomal protein S12, thereby affecting ribosomal biogenesis. Because RimP is a highly conserved mycobacterial protein, the understanding of its mechanism will provide insight in studying ribosomal biogenesis and developing new drugs to target *M. tuberculosis*.

Results

The crystal structure of MSMEG_2624

MSMEG_2624 was purified as a monomer in solution (data not shown). The crystal structure of MSMEG_2624 was solved by single isomorphous replacement with anomalous scattering (SIRAS) phasing, and the final model was refined to 2.2 Å (Fig. 1*A*). Detailed statistics of data processing, phasing, structure refinement, and Ramachandran plot are shown in Table 1 and Fig. S2. Both N-terminal (aa[4] 1–93) and C-terminal (aa 94–181) domains of MSMEG_2624 are similar to that of SP14.3, with 2.1 and 2.8 Å Cα root mean square deviation, respectively. The C-terminal domains of MSMEG_2624 and SP14.3 resemble the Sm fold, which is composed of six β sheets. The electron density of the loop between α2 and β3 is missing, which indicates a disordered structure (Fig. S3). The major difference between MSMEG_2624 and SP14.3, however, lies in the additional α-helix (α2′), connected by the long loop to the last β sheet β6′

[4] The abbreviations used are: aa, amino acids; NCS, noncrystallographic symmetry; AGC, automatic gain control.

Table 1

Crystal data processing, phasing and structure refinement statistics

In the two column results, the left column gives the raw count, right column gives the percentage.

Crystal	Native	K$_2$PtCl$_4$-derivative
Data Processing		
Space group	$P2_12_12_1$	$P2_12_12_1$
Unit-cell parameters (Å)	a=55.99	a=56.49
	b=75.44	b=74.94
	c=109.99	c=110.10
X-ray source	Rigaku FR-E+	Rigaku FR-E+
Detector	R-AXIS IV++ IP detector	R-AXIS IV++ IP detector
Wavelength (Å)	1.54187	1.54187
Resolution (Å)	39.22-2.2(2.32-2.2)	37.47-2.7(2.85-2.7)
No. of observed reflections	160233	45515
No. of unique reflections	24283	11115
Multiplicity	6.6(6.5)	3.9(3.7)
Completeness (%)	100(100)	88.0(91.4)
Mean $\langle I \rangle / \langle \sigma(I) \rangle$	14.4(3.5)	6.8(1.8)
R_{sym} (%)	5.6(37)	8.4(44.8)
Crystal mosaicity (°)	1.66	1.97
SIRAS phasing		
R_{iso}	0.297	
Resolution (Å)	37.47-2.7	
No. of heavy atoms in asymmetric unit	5	
Phasing power (overall/ano)	0.9214/1.8065	
<FOM> (initial/after SOLOMON)	0.393/0.487	
Asymmetric unit content	2 subunits	
Refinement Statistics		
Resolution range for refinement (Å)	39.22-2.2	
R factor (%)	23.11	
R_{free} factor (%)	26.25	
Number of water molecules	114	
Rmsd bond lengths (Å)	0.009	
Rmsd bond angles (°)	1.239	
MolProbity Statistics		
All-Atom Contacts	Clashscore, all atoms:	4.88	98thpercentile*(N=456, 2.20Å ± 0.25Å)
	Clashscore is the number of serious steric overlaps (> 0.4 Å) per 1000 atoms.		
Protein Geometry	Poor rotamers	7 / 2.57%	Goal: <0.3%
	Favored rotamers	252 / 92.65%	Goal: >98%
	Ramachandran outliers	0 / 0.00%	Goal: <0.05%
	Ramachandran favored	329 / 98.50%	Goal: >98%
	MolProbity score^	1.57	98thpercentile*(N=10167, 2.20Å ± 0.25Å)
	Cβ deviations >0.25Å	0 / 0.00%	Goal: 0
	Bad bonds:	0 / 2574 / 0.00%	Goal: 0%
	Bad angles:	0 / 3490 / 0.00%	Goal: <0.1%
Peptide Omegas	Cis Prolines:	2 / 16 / 12.50%	Expected: ≤1 per chain, or ≤5%

* 100thpercentile is the best among structures of comparable resolution; 0thpercentile is the worst. For clashscore the comparative set of structures was selected in 2004, for MolProbity score in 2006.

^ MolProbity score combines the clashscore, rotamer, and Ramachandran evaluations into a single score, normalized to be on the same scale as X-ray resolution.

(aa 158–165) on the C terminus of MSMEG_2624, which forms the handle of the barrel-like Sm fold (Fig. 1, *B* and *C*).

Despite the high resemblance between the crystal structure of MSMEG_2624 and the solution structure of SP14.3 at the individual domain level, they differ in the interdomain orientation. Whereas the solution structure of SP14.3 did not reveal a rigid orientation from the NOE data, our crystal structure of MSMEG_2624 shows strong electron density around the interdomain linker, indicating a well-defined clamplike orientation in the crystal (Fig. 1*D*). Under this orientation, the handle-like structure from the C-terminal domain interacts with the N-terminal domain through 1) hydrophobic interaction between the side chains of Phe-161 and Val-50 and 2) the hydrogen bond network formed among the Ser-162, Asp-35, and Val-36 (Fig. 1, *E* and *F*). These interactions are absent in the structure of SP14.3 and might be involved in the stabilization of the interdomain orientation, resulting in a more rigid structure. It is unclear whether the interdomain orientation is also present in solution, as we observed that both domains of MSMEG_2624 participated in crystal contact with the neighboring molecule (Fig. S4), which is expected for a protein that consists of only two domains.

The interdomain linker of MSEMG_2624 is essential for the coordinated binding with RpsL

To study the function of each domain of MSEMG_2624 in ribosome biogenesis, we first tested their interaction with binding partners. In previous interaction network studies of *E. coli* and *Helicobacter pylori*, RimP was reported to interact with S5, S7, and S12 of the small ribosomal subunit (10). In *M. smegmatis*, we detected the interaction between MSMEG_2624 and RpsL (S12) by co-immunoprecipitation followed by tandem MS (Fig. S5) and further validated it using a tandem affinity purification assay with recombinant proteins (Fig. 2*A*). We found that neither the C- nor the N-terminal domain of MSMEG_2624 alone is sufficient to bind RpsL (Fig. 2, *B* and *C*), which suggested that the two domains of MSEMG_2624 cooperatively interact with RpsL. In addition, the first 25 residues of RpsL were dispensable for the binding to MSMEG_2624 (Fig. S6).

We hypothesized that the linker region was essential for the coordination between the two domains of MSMEG_2624 to bind RpsL (Fig. 3*A*). To test this hypothesis, we mutated residues in this region and tested their effects on binding with RpsL. The charged residues, Asp-93 and Arg-94, were either deleted or reversed/neutralized; residues with more (Pro-95) or less (Gly-91) restricted torsion angles were swapped (Fig. 3*A* and Fig. S7). As shown in Fig. 3*B*, both linker deletion mutants significantly reduced the binding efficiency to RpsL, suggesting the importance of the linker region. The swapping of glycine to proline at position 91 but not 95 abolished the binding. We speculate that this distinct effect might be explained by the fact that G91P mutant disrupted the interdomain orientation by steric hindrance, whereas P95G merely increased the flexibility of the backbone. Alternatively, the residue Gly-91 might directly interact with RpsL. For mutations on the charged residues, R94D/A but not D93R/A greatly reduced the strength of the binding. In addition, we noticed that R94D showed a much stronger effect than R94A, suggesting

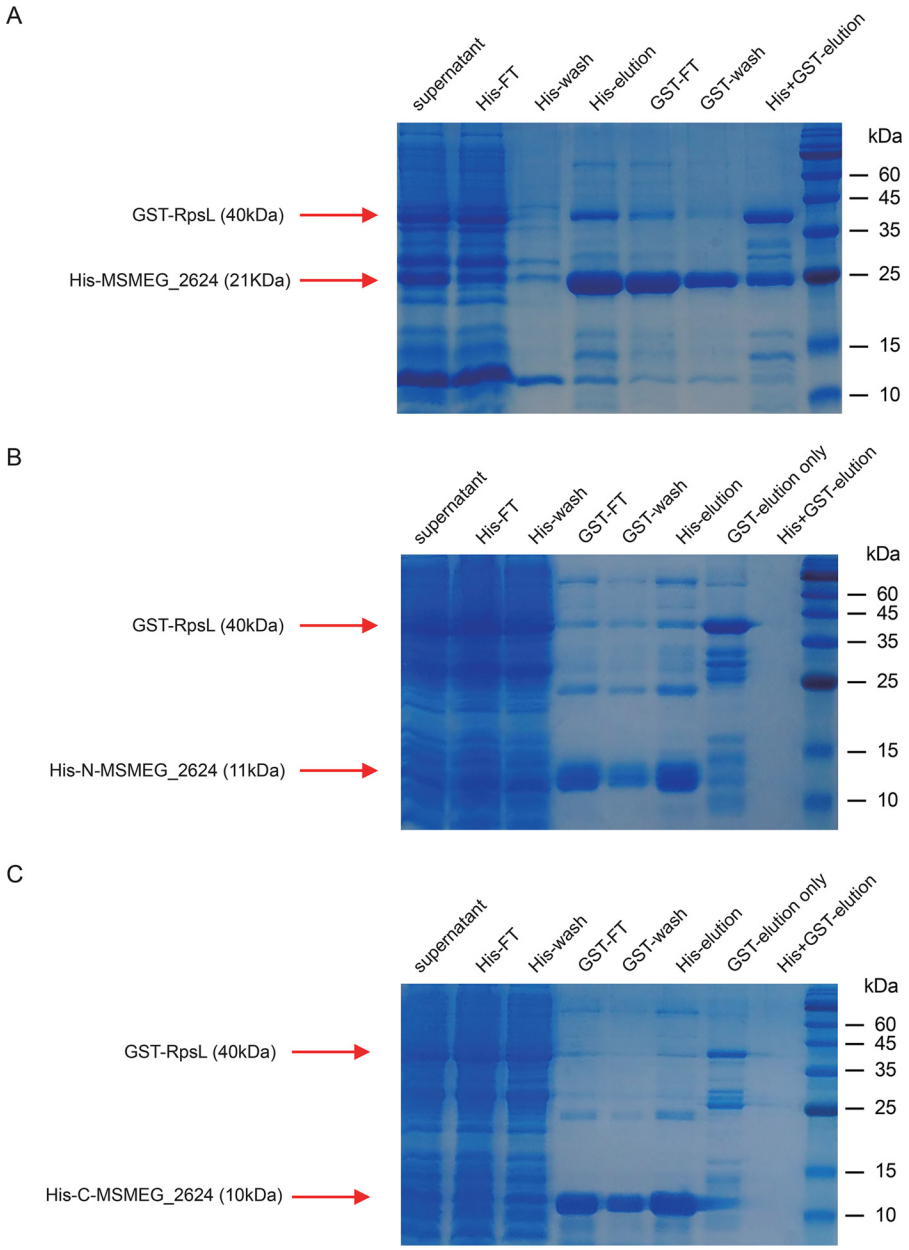

Figure 2. Tandem affinity purification maps the MSMEG_2624–RpsL interaction. His-MS- MEG_2624 (*A*) or His-tagged individual MSMEG_2624 domains (*B* and *C*) and GST-RpsL were recombinantly co-expressed and purified through Ni^{2+} and then GST affinity purification. The fractions are *labeled* at the *top* of the corresponding *lanes* (*FT*, flow-through; *GST-FT/wash/elution*, GST affinity chromatography of fractions after the first His elution; *GST-elution only*, elution using the GST affinity chromatography without the Ni^{2+} affinity chromatography). *Red arrows* mark where the corresponding proteins are expected.

that the positive charge of Arg-94 might directly participate in binding with RpsL through electrostatic interaction. To test whether the decreased binding efficiency of the mutants was due to protein denaturation or aggregation, we used size-exclusion chromatography to measure their molecular size. We found that all mutants had similar elution profiles as the WT, suggesting their proper folding (Fig. S8). The linker region is significantly enriched for highly conserved residues ($p = 0.0005$, Fisher exact test), suggesting its functional importance. Strikingly, we observed that all mutants that affected conserved residues showed a decrease in binding efficiency with RpsL, which suggested that these sites were under purifying selections. Taken together, we demonstrated that the linker of MSMEG_2624 was essential in coordinating the two domains to bind with RpsL.

The interdomain linker of MSMEG_2624 is essential for ribosomal biogenesis

Although previous literature suggested that RimP was involved in the maturation of the 30S ribosome by stabilizing the pseudoknot structure and facilitating the incorporation of late binder ribosomal proteins, a detailed mechanism is still lacking. Having shown the importance of interdomain linker of MSMEG_2624 in binding RpsL, we analyzed the functions of RimP in ribosomal biogenesis in terms of its interaction with

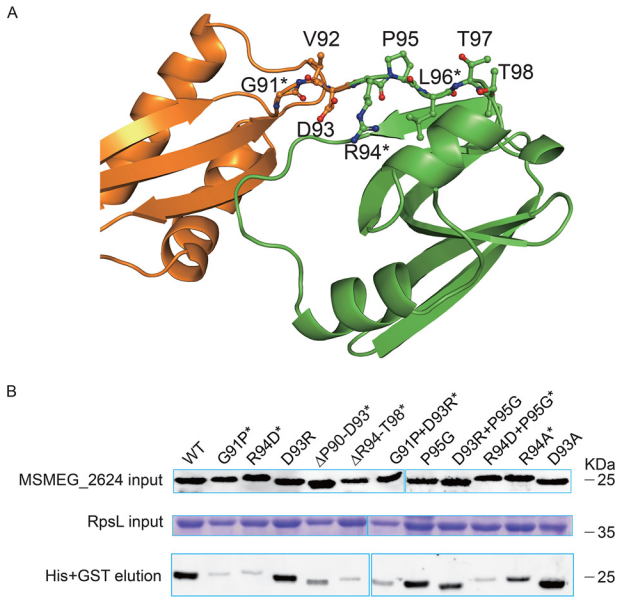

Figure 3. Site-directed mutagenesis on the linker region of MSMEG_2624 and the effects on MSMEG_2624–RpsL interaction. *A*, crystal structure of the linker region of MSMEG_2624. Evolutionarily conserved residues are marked by an *asterisk*. *B*, pulldown assay determines the binding efficiency between GST-RpsL and His-tagged MSMEG_2624 and its mutants. *Top*, Western blot (anti-His antibody) detects the input amount of His-MSMEG_2624 after the first Ni^{2+} affinity chromatography. *Middle*, Coomassie staining detects the input amount of GST-RpsL after the second GST affinity chromatography. *Bottom*, Western blot (anti-His antibody) detects the amount of eluted His-MSMEG_2624 after the second GST affinity chromatography. *Asterisks* mark the evolutionarily conserved residues. *Cyan rectangular boxes* mark where the gels/blots are cropped from the original ones. Images of cropped blots (*top* and *bottom*) are aligned by the same loading control of the purified His-MSMEG_2624 protein (not shown), whereas those of cropped gels (*middle*) are aligned by the protein ladder (not shown).

RpsL. Similarly to RimP in *E. coli*, MSMEG_2624 knockout in *M. smegmatis* showed reduction in polysomes and 70S ribosomes and concomitantly increased free 30S and 50S ribosomal subunits (Fig. 4*A*). The phenotype can be rescued by complementation of RimP in the knockout strain (Fig. 4*A*). In addition, we confirmed using MS that MSMEG_2624 was essential for the efficient recruitment of RpsL to the maturing 30S subunit (Fig. 4*B*). To specifically characterize the *in vivo* effects of the linker region of MSMEG_2624 on ribosomal biogenesis, we analyzed the ribosomal profile of the MSMEG_2624 knockout strains of *M. smegmatis*, complemented by two MSMEG_2624 mutants. We compared one that significantly abolished the interaction with RpsL (ΔP90–D93), with another that did not (P95G). The knockout strain complemented by the ΔP90–D93 mutant showed a significantly lower level of 70S ribosome than that complemented by P95G, suggesting that the interdomain linker of MSMEG_2624 is essential for ribosome biogenesis via its interaction with RpsL (Fig. 4*C*). Taken together, we propose a model of ribosomal biogenesis in which the two domains of RimP cooperatively bind with S12 through the linker region, whereby it facilities efficient maturation of the complete 70S ribosome.

Discussion

In this study, we have reported a high-resolution crystal structure of RimP homolog in *M. smegmatis* that revealed a well-defined interdomain orientation. Moreover, we have provided a mechanistic view of RimP in ribosomal biogenesis. Our binding assays demonstrate that the two domains of RimP cooperatively bind with the small ribosomal protein RpsL through its linker region. More importantly, this linker region is essential for ribosomal biogenesis. Sashital *et al.* (8) reported that in the absence of RimP, the central pseudoknot structure of rRNA was unstable, resulting in the accumulation of intermediates. These intermediate products were depleted of S5 and S12, which are both pseudoknot-interacting ribosomal proteins. We propose that the linker region of RimP forms a platform for recruiting S12 and facilitating the rRNA binding. Indeed, this hypothesis could explain the functional importance of the evolutionarily conserved residues in this linker region.

In the structure of MSMEG_2624 and SP14.3, the C-terminal domain has an Sm fold that is also observed in Hfq, an RNA chaperone that mediates the interaction between sRNAs and their mRNA targets. Hfq is a hexamer that efficiently binds RNA, whereas RimP remains as a monomer in solution and does not appear to show RNA-binding activity. Indeed, the amino acid sequence between Hfq and RimP diverges significantly. This observation indicates that Hfq and the C-terminal domain of RimP are functionally divergent, even though they are structurally similar.

RimP is highly conserved in prokaryotes, and its functional importance in ribosomal biogenesis has been reported in multiple bacterial species. As no homolog protein has been identified in mammals, it has the potential of becoming a drug target for therapeutic purposes to combat bacterial infections, such as tuberculosis. This makes our structure and biochemical study of particular importance for future drug design.

Experimental procedures

Bacterial strains and plasmids

The bacterial strains and vectors used in this work are summarized in Table S1.

Protein expression, purification, and crystallization

Recombinant His-tagged MSMEG_2624 was expressed in *E. coli* BL21 (DE3) cells, and purified using nickel-nitrilotriacetic acid affinity chromatography. The His tag was cleaved, and the protein was further purified by size-exclusion chromatography (10 mM Tris-HCl, pH 7.4, 250 mM NaCl). MSMEG_2624 crystals were grown under 20% PEG 3350, 6% acetonitrile, 0.2 M sodium citrate (pH 8.0) by the hanging-drop vapor-diffusion method at 16 °C. The native crystals were cryoprotected by quickly passing through the crystallization buffer containing 12% glycerol before flash freezing. Heavy atom soaking was performed by directly adding 40 mM K_2PtCl_4 water solution to crystals in the mother liquor twice with a 15-min interval between, to a final concentration of ~20 mM. The crystals were soaked in the dark overnight and back-soaked for 5 min in cryoprotectant buffer containing 8.8 mM K_2PtCl_4 and 12% glycerol before data collection.

Structure determination

Data sets were processed using the CCP4 suite (11). Specifically, data were integrated using iMosflm version 1.5 and merged and scaled using SCALA. Scailit was used to scale across the data sets after they were combined using CAD.

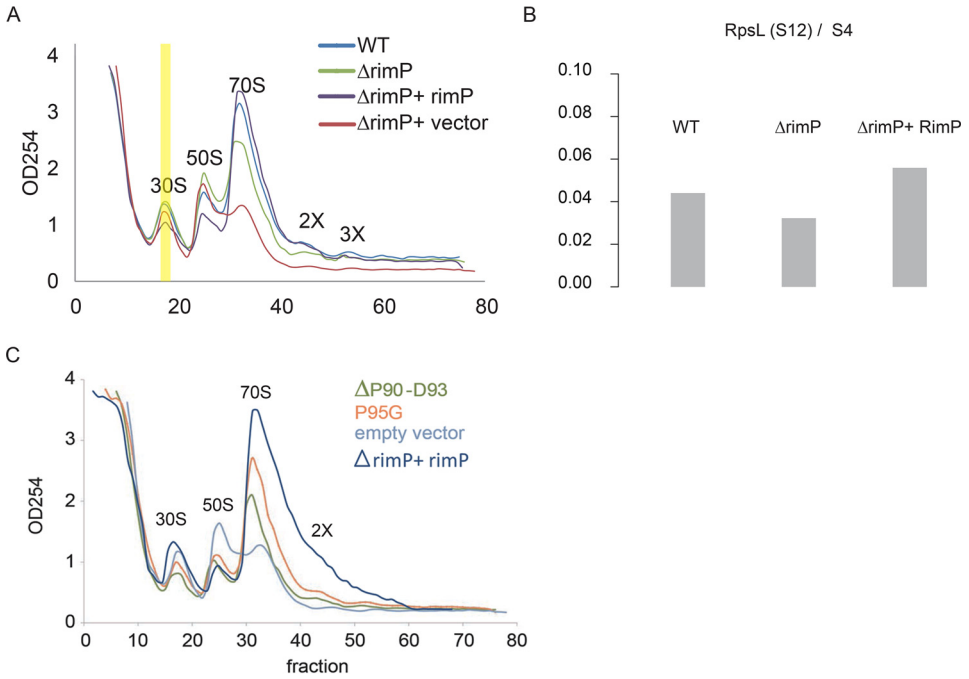

Figure 4. The efficiency of *in vivo* ribosomal biogenesis of MSMEG_2624 mutants. *A*, sucrose gradient centrifugation of the WT *M. smegmatis*, the MSMEG_2624 knockout strain, the MSMEG_2624 knockout with the vector that expresses MSMEG_2624, and the MSMEG_2624 knockout that carries the empty vector. The *vertical yellow bar* marks the fraction further characterized using MS in *B*. *B*, The bar plot shows the ratio of S12/S4 in the 30S subunit of WT, the MSMEG_2624 deletion mutant strain, and the MSMEG_2624 knock-out strain with the vector that expresses MSMEG_2624. *C*, sucrose gradient centrifugation shows the ribosome profile of the MSMEG_2624 mutants which affects binding with RpsL (ΔP90-D93, shown in green), and which does not (P95G, shown in red). The controls of empty vector and empty vector + WT are shown in cyan and purple.

Heavy atom sites were searched using Afro/Crunch2 followed by refining/phasing using Bp3 using the CRANK suite (12). The initial map was built by the automated model building software Buccaneer (13), followed by iterative local noncrystallographic symmetry (NCS) phased refinement using DM (14) and Refmac (15). Local NCS operator was only used in early stages of refinement to help identify the initial phase. After the refinement statistics converged in the Refmac program, we used Phenix refinement (16) and manual building using the molecular graphics program COOT (17), without the use of NCS. Structures were visualized using PyMOL (18). Statistics of the quality of the structure were calculated using MolProbity (19). Statistics of crystal contacts were calculated using Pisa analysis (20). The structure was deposited to the Protein Data Bank (entry 5GL6).

Construction of MSMEG_2624 knockout strain (ΔrimP)

The rimP null mutant strain (Δ*rimP*) was constructed using homologous recombination to replace the *rimP* gene with the hygromycin selection marker as described previously (21). Briefly, a DNA substrate for allelic replacement of *rimP* (MSMEG_2624) was generated by cloning 500-bp upstream and downstream regions of the *rimP* gene to 5′ and 3′ ends of the hygromycin (*hyg*) gene, respectively, and transformed into the Msmeg mc^{2}155 strain harboring a pJV53 vector, which can produce recombinase for efficient recombination. The successful knockout strain Δ*rimP::hyg* was selected and confirmed by sequencing and Western blot analysis.

In vitro binding of recombinant RimP (MSMEG_2624) and RpsL

Plasmids pGEX-6P-1-RpsL and pRsfDuet-1-RimP were co-transformed to *E. coli* BL21(DE3). The bacteria were grown in 3 liters of Luria–Bertani medium at 37 °C until A_{600} ~0.6. Protein expression was induced by the addition of 1 mM isopropyl 1-thio-β-D-galactopyranoside at 16 °C overnight. Bacteria were harvested and resuspended in 1× PBS and 0.5% Triton X-100. Bacteria were lysed by sonication, and cell debris and precipitants were removed by centrifugation. The supernatant was mixed with TALON Cobalt beads (Clontech) for 1.5 h at 4 °C followed by 10 column bed volumes of 1× PBS washing. Proteins were then eluted with 20 mM Tris-HCl, 500 mM NaCl, 250 mM imidazole. The eluted protein was incubated with GSH column (GE Healthcare) for 1.5 h at 4 °C and washed with 10 column bed volumes of 1× PBS. Proteins were eluted with 20 mM Tris-HCl, 150 mM NaCl, and 10 mM reduced GSH.

Polysome profiling

The strains *WT, ΔrimP, ΔrimP+rimP, and ΔrimP+*vector were cultured in 7H9 medium, and the cells were harvested at early log phase (A_{600} ~1). The cell pellets were lysed as described previously, and the ribosome was extracted according to the method reported previously (22).

Mass spectrometry study of ribosomal fractions

Sample preparation—The fraction was precipitated in acetone with a 1:4 ratio at −20 °C overnight. The protein pellet was dissolved in urea buffer (8 M urea in 50 mM ammonium bicarbonate). Protein concentration was measured by a Bradford assay. 10 μg of protein were diluted to 1 M urea by 50 mM ammonium bicarbonate and digested overnight at 37 °C using sequencing grade trypsin (Promega) with an enzyme/substrate ratio of 1:50. 5 μg of peptide were desalted by C18 Ziptip (Mil-

lipore). The sample pellet was reconstituted in formic acid and injected into MS.

LC-MS/MS experiment—The obtained peptides were reconstituted in 12 μl of 0.1% formic acid, and 2 μl was injected into an Easy-nLC 1200 (Thermo). Peptides were separated on a reverse phase C18 column (75-μm inner diameter $\times$ 15 cm, 3-μm particle size) and analyzed by an Orbitrap mass spectrometer (Thermo). The mobile phase buffer consisted of 0.1% formic acid in ultrapure water (buffer A) with an eluting buffer of 0.1% formic acid in 80% (v/v) acetonitrile (buffer B) run with a linear 50-min gradient of 7–25% buffer B at a flow rate of 250 nl/min. The mass spectrometer was operated in positive ion mode acquiring a survey mass spectrum with a mass resolution of 120,000, m/z = 350–1800 using an automatic gain control (AGC) target of 3 $\times$ 106. The 12 most intense ions were selected for higher-energy collisional dissociation fragmentation (normalized collision energy 27), and MS/MS spectra were generated with an AGC target of 1 $\times$ 105 at a resolution of 30,000. The dynamic exclusion time was set to 30 s.

Database analysis—The raw data from MS/MS spectra were searched against the *M. smegmatis* strain mc2 155 (downloaded on August 20, 2018) using the Sequest HT node integrated within the Proteome Discoverer (PD) software (version 2.2, Thermo). The precursor and fragment mass tolerances were set to 10 ppm and 0.02 Da, respectively. A maximum of two missed cleavages was allowed for trypsin digestion. Cysteine carbamidomethylation was set as static modification, whereas methionine oxidation and N-terminal acetylation were set as variable modifications. False discovery rates of peptide spectrum matches and identified peptides were determined using the Percolator algorithm at 1% based on q value. For quantification, the precursor ion areas in a node-based processing and consensus workflow in PD 2.2 were used. The areas of the ions in the MS1 scan were calculated using the Minora Feature alignment and feature mapping. The abundance values of proteins were obtained via a label-free quantification method using LC-MS/MS.

Author contributions—T. C. and T. C. K. L. conceptualization; T. C., X. W., C. O. K. L., H.-K. K., J. L., S. L., H. Q. P., R. W., L. Z., and R. Y. T. K. data curation; T. C. and T. C. K. L. formal analysis; T. C. visualization; T. C., X. W., and C. O. K. L. methodology; T. C. writing-original draft; T. C. and T. C. K. L. writing-review and editing; X. W., C. O. K. L., and J. C. K. N. investigation; K.-F. L., J. C. K. N., and T. C. K. L. resources; J. C. K. N. and T. C. K. L. supervision; T. C. K. L. validation; T. C. solving the crystal structure.

Acknowledgments—We thank Professor Yibei Xiao for discussion of structural analysis and Lauren A. Choate, Dr. Wendy Kwok, and Paul R. Munn for helpful discussion of the manuscript.

References

1. Neidhardt, F. C., Ingraham, J. L., and Schaechter, M. (1990) *Physiology of the Bacterial Cell: A Molecular Approach*, p. 520, Sinauer Associates Inc., Sunderland, MA
2. Nierhaus, K. H., and Dohme, F. (1974) Total reconstitution of functionally active 50S ribosomal subunits from *Escherichia coli*. *Proc. Natl. Acad. Sci. U.S.A.* **71,** 4713–4717 CrossRef Medline
3. Champney, W. S. (1977) Kinetics of ribosome synthesis during a nutritional shift-up in *Escherichia coli* K-12. *MGG Mol. Gen. Genet.* **152,** 259–266 CrossRef Medline
4. Nord, S., Bylund, G. O., Lövgren, J. M., and Wikström, P. M. (2009) The RimP protein is important for maturation of the 30S ribosomal subunit. *J. Mol. Biol.* **386,** 742–753 CrossRef Medline
5. Chang, J., Pang, E., He, H., and Kwang, J. (2008) Identification of novel attenuated *Salmonella enteritidis* mutants. *FEMS Immunol. Med. Microbiol.* **53,** 26–34 CrossRef Medline
6. Yu, L., Gunasekera, A. H., Mack, J., Olejniczak, E. T., Chovan, L. E., Ruan, X., Towne, D. L., Lerner, C. G., and Fesik, S. W. (2001) Solution structure and function of a conserved protein SP14.3 encoded by an essential *Streptococcus pneumoniae* gene. *J. Mol. Biol.* **311,** 593–604 CrossRef Medline
7. Bunner, A. E., Nord, S., Wikström, P. M., and Williamson, J. R. (2010) The effect of ribosome assembly cofactors on *in vitro* 30S subunit reconstitution. *J. Mol. Biol.* **398,** 1–7 CrossRef Medline
8. Sashital, D. G., Greeman, C. A., Lyumkis, D., Potter, C. S., Carragher, B., and Williamson, J. R. (2014) A combined quantitative mass spectrometry and electron microscopy analysis of ribosomal 30S subunit assembly in *E. coli*. *Elife* **3,** 10.7554/eLife.04491 CrossRef Medline
9. World Health Organization (2016) *WHO Global Tuberculosis Report 2016*, World Health Organization, Geneva
10. Kerrien, S., Aranda, B., Breuza, L., Bridge, A., Broackes-Carter, F., Chen, C., Duesbury, M., Dumousseau, M., Feuermann, M., Hinz, U., Jandrasits, C., Jimenez, R. C., Khadake, J., Mahadevan, U., Masson, P., *et al.* (2012) The IntAct molecular interaction database in 2012. *Nucleic Acids Res.* **40,** D841–D846 CrossRef Medline
11. Winn, M. D., Ballard, C. C., Cowtan, K. D., Dodson, E. J., Emsley, P., Evans, P. R., Keegan, R. M., Krissinel, E. B., Leslie, A. G. W., McCoy, A., McNicholas, S. J., Murshudov, G. N., Pannu, N. S., Potterton, E. A., Powell, H. R., *et al.* (2011) Overview of the CCP4 suite and current developments. *Acta Crystallogr. D Biol. Crystallogr.* **67,** 235–242 CrossRef Medline
12. Ness, S. R., de Graaff, R. A. G., Abrahams, J. P., and Pannu, N. S. (2004) Crank: new methods for automated macromolecular crystal structure solution. *Structure* **12,** 1753–1761 CrossRef Medline
13. Cowtan, K. (2006) The Buccaneer software for automated model building. *Acta Crystallogr. D Biol. Crystallogr.* **62,** 1002–1011 CrossRef Medline
14. Cowtan, K. (1999) Error estimation and bias correction in phase-improvement calculations. *Acta Crystallogr. D Biol. Crystallogr.* **55,** 1555–1567 CrossRef Medline
15. Murshudov, G. N., Vagin, A. A., and Dodson, E. J. (1997) Refinement of macromolecular structures by the maximum-likelihood method. *Acta Crystallogr. D Biol. Crystallogr.* **53,** 240–255 CrossRef Medline
16. Adams, P. D., Afonine, P. V., Bunkóczi, G., Chen, V. B., Davis, I. W., Echols, N., Headd, J. J., Hung, L. W., Kapral, G. J., Grosse-Kunstleve, R. W., McCoy, A. J., Moriarty, N. W., Oeffner, R., Read, R. J., Richardson, D. C., *et al.* (2010) PHENIX: a comprehensive Python-based system for macromolecular structure solution. *Acta Crystallogr. D Biol. Crystallogr.* **66,** 213–221 CrossRef Medline
17. Emsley, P., and Cowtan, K. (2004) Coot: model-building tools for molecular graphics. *Acta Crystallogr. D Biol. Crystallogr.* **60,** 2126–2132 CrossRef Medline
18. DeLano, W. L. (2015) *The PyMOL Molecular Graphics System*, version 1.8, Schrödinger LLC, New York
19. Chen, V. B., Arendall, W. B., 3rd, Headd, J. J., Keedy, D. A., Immormino, R. M., Kapral, G. J., Murray, L. W., Richardson, J. S., and Richardson, D. C. (2010) MolProbity: all-atom structure validation for macromolecular crystallography. *Acta Crystallogr. D Biol. Crystallogr.* **66,** 12–21 CrossRef Medline
20. Krissinel, E., and Henrick, K. (2007) Inference of macromolecular asssemblies from crystalline state. *J. Mol. Biol.* **372,** 774–797 CrossRef Medline
21. van Kessel, J. C., and Hatfull, G. F. (2007) Recombineering in *Mycobacterium tuberculosis*. *Nat. Methods* **4,** 147–152 CrossRef Medline
22. Bylund, G. O., Wipemo, L. C., Lundberg, L. A. C., and Wikström, P. M. (1998) RimM and RbfA are essential for efficient processing of 16S rRNA in *Escherichia coli*. *J. Bacteriol.* **180,** 73–82 Medline